Dihydrogen H_2 steady state in α-radiolysis of water adsorbed on PuO_2 surface

Laurent Venault, Arnaud Deroche, Jérémy Gaillard, Olivier Lemaire, Natalia Budanova, Jackie Vermeulen, Jérôme Maurin, Nicolas Vigier, Philippe Moisy

Dihydrogen H_2 steady state in α-radiolysis of water adsorbed on PuO_2 surface

Laurent Venault[a,*], Arnaud Deroche[a], Jérémy Gaillard[a], Olivier Lemaire[a], Natalia Budanova[a], Jackie Vermeulen[a], Jérôme Maurin[a], Nicolas Vigier[b], Philippe Moisy[a]

[a] CEA, Nuclear Energy Division, Research Department on Mining and Fuel Recycling Processes, BP 17171 F-30207 Bagnols-sur-Cèze, France

[b] ORANO, 1 place Jean Millier, 90084 Paris La Défense, France

* coresponding author : laurent.venault@cea.fr, +33 4 66 79 18 45

Abstract

Radiolysis of water adsorbed on PuO_2 surface has been the subject of several studies but still remains poorly understood. The present study brings new experimental results helping to further understand the phenomena occurring at PuO_2 surface. Radiolysis of adsorbed water on PuO_2 surface leads to the reach of a steady state in hydrogen content when relative humidity is kept constant implying an equilibrium between generation and consumption of hydrogen. The influences of specific surface area, relative humidity, PuO_2 dose rate and composition of the atmosphere (Ar *vs* air) on hydrogen generation were investigated. A significant evolution of the hydrogen generation kinetics was observed upon PuO_2 surface aging. This result might be related to an evolution of the surface physicochemical state induced by a long-term storage in $H_2O/H_2/O_2$ atmosphere. The surface evolution modifies the equilibrium between generation and consumption of hydrogen. Several annealing thermal treatment were necessary to retrieve H_2 accumulations kinetics similar to the ones obtained with the same sample as freshly prepared. This indicates an important evolution of PuO_2 surface and subsurface. A mechanism is described to explain the surface evolution and its effect on H_2 accumulation through radiolysis of adsorbed water.

Highlights

- H_2 formed under α-radiolysis of water sorbed on PuO_2 surface reaches a steady state after several days.
- The initial rate R_0 increases with dose rate, relative humidity and specific surface area.
- H_2 steady-state concentration increases with dose rate, relative humidity and specific surface area.
- Hydrogen accumulation and consumption reach the same steady state and conduct to a kinetic model.
- The rates of hydrogen accumulation increase with long term storage and is restored by annealing treatments.

Keywords

alpha radiolysis, plutonium dioxide, surface, water, hydrogen

1 - Introduction

Plutonium dioxide is known to be the most stable compounds of plutonium and is then dedicated to plutonium handling under aerobic conditions. It is well known for a long time that the water, adsorbed on the surface, can be decomposed by radiolysis under the effect of alpha particles emitted by plutonium leading to generation of hydrogen (Hodkin, 1965). Moreover, plutonium dioxide is known as a hygroscopic compound and water can be adsorbed to an extent of 2- 3 wt% (Stakebake, 1973; Benhamou, 1980). Water adsorption on plutonium dioxide is described as a three stages mechanism (Stakebake, 1973). The first monolayer is chemisorbed on the surface. Water chemisorption consists in water decomposition and formation of hydroxyl group on the surface. The second stage is called "quasi-chemisorption" and results in water molecules strongly bonded to the hydroxyl groups by H-bonding. The last stage is called physisorption and leads to weakly bonded water molecules. Several monolayers of water can adsorb on top of the two first monolayers. Recent work indicates that the very top layers are in close physical state to free water shown by an adsorption enthalpy closed to condensation heat of water (Alexandrov, 2011). These three type of water adsorption on plutonium dioxide surfaces can be discriminated by their desorption temperature. Physisorbed water is evacuated under vacuum at temperature below 200°C. The "quasi-chemisorbed" water requires temperature around 500°C to fully desorb. Finally the chemisorbed water requires temperature higher than 800°C to obtain efficient desorption (Stakebake, 1973).

In the case of plutonium, the alpha particles emitted by the material could lead to an internal alpha radiolysis. Different experimental studies were performed on hydrogen generation through radiolysis of water adsorbed on PuO_2 (Vladimirova, 2002; Duffey, 2002; Sims, 2013). In the case of PuO_2, an estimation of energy redistribution between PuO_2 and adsorbed water is very difficult, because of many parameters governing water sorption. Different methodologies were used. Vladimirova *et al.* contacted plutonium dioxide pellets or powder samples with a defined amount of liquid water and then the hydrated samples were put in closed cells (Vladimirova, 2002). Hydrogen and oxygen generation was followed using gas phase chromatography versus dose rate using plutonium from reprocessing of fuel assemblies with different burnups. Radiolysis leads to uncommonly high generation of both hydrogen and oxygen. Initially, both kinetics are linear versus time and curve slopes increase with humidity content and dose rate (Vladimirova, 2002). After long experiment time, around a hundred days, the amount of hydrogen reaches a steady value corresponding to approximately complete decomposition of the sorbed water. Other studies were performed in which plutonium dioxide was initially equilibrated with humid atmosphere and then placed into a sealed container (Duffey, 2002; Sims, 2013). Gas phase was also analyzed using gas phase chromatography. In these experiments, water adsorption is controlled by water partial pressure in equilibrium with amount of water adsorbed on the surface. Sample after equilibration into humid conditions are taken out and placed with a dry atmosphere. The first phenomenon occurring is equilibration of the gas phase water content and adsorbed water and water might desorb from the surface. On the other side, Duffey et al. observe non-systematic oxygen generation (Duffey, 2002). Hydrogen and oxygen generations are both observed only when hydrogen generation is high. Experimental results from these studies also suggest the ability of PuO_2 surface to catalyze the recombination of hydrogen and oxygen to form water since it was shown the pressure of

H_2/O_2 mixture contacted with PuO_2 is decreasing. Recently, a study was performed on plutonium dioxide using an experimental device with constant relative humidity (Sims, 2013). The results show a relation between hydrogen generation and relative humidity. Hydrogen generation appears linear versus time over more than 15 days and no steady state was observed. Also Hydrogen accumulation rate appears to increase with relative humidity. Literature presents different approaches to study the phenomena occurring at plutonium dioxide surface upon water adsorption but the mechanism is still poorly understood.

This water, adsorbed into the surface, could lead to the formation of dihydrogen by chemical surface reactivity. The studies of Haschke *et al.* bring interesting results on hydrogen generation during plutonium dioxide storage (Haschke, 2001). In this study, no oxygen generation was observed leading to the controversial assumption of PuO_{2+x} (eq. 1).

$$PuO_2 + xH_2O_{(ads)} \rightarrow PuO_{2+x\,(s)} + xH_{2\,(g)} \qquad (1)$$

In the same work, these authors suggest that in the presence of a mixture of H_2 and O_2, plutonium dioxide surface can catalyze the H_2 and O_2 combination with intermediate formation of water. This latter leads to the formation of PuO_{2+x} by water-catalyzed reaction of PuO_2 and O_2 (eq. 2 and 3).

$$H_{2(ads)} + 1/2O_{2(ads)} \rightarrow 2H_{(ads)} + O_{(ads)} \rightarrow H_2O_{(ads)} \qquad (2)$$

$$PuO_{2(s)} + x/2O_{2(g)} \xrightarrow{H_2O\ (ads)} PuO_{2+x(s)} \qquad (3)$$

However, the chemical surface reactivity and the surface state are very difficult to probe. In fact, physisorbed water layers are weakly bonded to the surface and chemisorbed water layers could be altered by intrusive analytical technics (XPS, Raman).

Moreover, the calculation might only roughly estimate the effective dose adsorbed by water adsorbed on PuO_2 surface. Another difficulty arises from the estimation of the amount of water adsorbed on the surface. Dosage of accurate amount of water on a PuO_2 surface cannot lead to a perfectly known water content on PuO_2 surface (Stakebake, 1973; Benhamou, 1980; Haschke 1997). The different kind of adsorbed water might have a different behaviour toward radiolysis. Experimental work already suggested that the radiation yield differs from one water monolayer to the other (Laverne, 2002; Petrik, 2001). The radiolysis of the first monolayers of water would lead to higher hydrogen generation.

However, the method, proposed by Vladimirova et *al.* (Vladimirova, 2002), is based on the number of electrons and respective amount of H_2O and PuO_2 (Eq. 4).

$$D_{H_2O} = D_{PuO_2} \times \frac{10 \times m_{H_2O}}{110 \times m_{PuO_2}} \qquad \text{(Eq. 4)}$$

where D_{H2O} is the dose absorbed by water and D_{PuO2} the dose generated by PuO_2, 10 and 110 are the numbers of electrons in the molecules of these compounds, and m_{H2O} and m_{PuO2} are the numbers of moles of H_2O and PuO_2. This equation is used by Vladimirova to calculate hydrogen yield from hydrogen content kinetics.

The radiolysis of water adsorbed on non-radioactive oxide surface differs from radiolysis of bulk free water (Laverne, 2002). The H_2 radiolytic yield in alpha radiolysis of free water was determined to be equal to 1.25 x

10^{-7} mol J^{-1} (Laverne, 2000; Allen, 1961). In the case of oxide interface, the presence of this interface leads to redistribution of absorbed radiation energy (Petrik, 2001). This phenomenon induces a higher hydrogen generation from water molecule decomposition compared to free water radiolysis (Laverne, 2002; Petrik, 2001; Laverne, 2003). Energy absorbed by solid material is partially redirected toward the adsorbed water. The chemical interface oxide nature appears to be an important criterion for promoting hydrogen generation upon radiation and the oxide band gap energy is a key factor. Radiolysis promoters appear to have band gap within the range from 4.5 to 6eV (Petrik, 2001). Plutonium dioxide band gap energy was experimentally measured at 1.8eV (McNeilly, 1964), and its ability to promote hydrogen generation should be quite low. A mechanism explaining energy redistribution has been proposed for water decomposition on Al_2O_3 surface (Eq. 5 and Eq. 6) (Petrik, 2001).

$$h^+ + H_2O \rightarrow H_2O^+ \xrightarrow{e^-} H_2O* \rightarrow H + OH \qquad \text{(Eq. 5)}$$

$$H + H \rightarrow H_2 \qquad \text{(Eq. 6)}$$

The formation of hole-electron pair in the oxide and the migration of the charge carrier to the surface could explain the energy transfer from the solid phase to the adsorbed phase. Other mechanisms were proposed for energy transfer: exciton transfer and dissociative electron attachment (Laverne, 2003). The calculation of radiation yield of hydrogen presents some difficulties in the case of adsorbed water. Radiation yields are based on the estimation of the amount of radiation energy absorbed by the material. The assessment of the absorbed dose is usually done on solid phase or liquid phase using experimental dose measurements.

The purpose of the present study is then to bring new experimental results in order to improve understanding of the complex phenomena of water radiolysis on plutonium dioxide surface. These studies bring interesting results on hydrogen generation during plutonium dioxide storage. The methodology focused on obtaining experimental conditions to limit sources of uncertainties. Plutonium dioxide samples were prepared on purpose with high purity and relative humidity was kept constant all along experiment in order to have a constant renewal of water on the surface.

2 - Experimental section

2.1 - Plutonium isotopy

Different dose rates were obtained using different plutonium isotopies as described in Table 1. Plutonium isotopy was obtained from Thermal Ionization Mass Spectroscopy analysis (TIMS) with the help of the CEA Marcoule Analysis Laboratory team. Plutonium isotopies were chosen with low ^{241}Pu content to limit β^- decay of this isotope and the subsequent participation of ^{241}Am α- and γ-radiolysis. Dose rate are calculated using the equation (Eq. 7) given by Vladimirova *et al.* (Vladimirova, 2002). Alpha energies and specific activities are obtained from LNHB database (see additional data, Table 9). Plutonium dioxide emitted dose rates are given in Table 1.

$$\dot{D}_{Pu} = 3.7 \times 10^{10} \left(\sum_i f_{i,\alpha} E_{i,\alpha} A_{i,\alpha} + \sum_i f_{i,\beta} E_{i,\beta} A_{i,\beta}\right) \quad \text{(Eq. 7)}$$

Where $f_{i,\alpha}$: Mass fraction of the isotope i for the α irradiations

$f_{i,\beta}$: Mass fraction of the isotope i for the β irradiations

$E_{i,\alpha}$: Energy of the α particle emitted by the isotope i (eV)

$E_{i,\beta}$: Energy of the β particle emitted by the isotope i (eV)

$A_{i,\alpha}$: Specific α activity of the isotope i ($Ci.g^{-1}$)

$A_{i,\beta}$: Specific β activity of the isotope i ($Ci.g^{-1}$)

The conversion factor 3.7 x 10^{10} is used to convert from curie (Ci) to becquerel ($disintegration.s^{-1}$).

The mean dose rate emitted per gram of PuO_2 ($MeV.g^{-1}.s^{-1}$) is obtained by multiplying the mean dose rate emitted per gram of Pu by the molar mass ratio M_{Pu}/M_{PuO2} (Eq. 8).

$$\dot{D}_{PuO2} = MPu/MPuO_2 \times \dot{D}_{Pu} \quad \text{(Eq. 8)}$$

Table 1 - Isotopic compositions of plutonium solutions and corresponding PuO_2 total dose rates.

Isotopy	^{238}Pu	^{239}Pu	^{240}Pu	^{241}Pu	^{242}Pu	Dose rate ($Gy.s^{-1}$)
I	--	96.92	2.98	0.03	0.08	1.8
II	0.17	76.51	21.23	1.41	0.68	3.5
III	0.69	70.14	22.33	3.86	2.98	6.3
IV	1.07	67.74	22.39	4.68	4.12	8.3
V	3.08	66.42	21.93	4.49	4.15	18.0
VI	6.58	64.08	21.01	4.20	4.18	35.0

Plutonium emitted dose rate were calculated using the initial isotopic composition of plutonium. However, the isotopic composition of samples can change over time due to the decay of plutonium and ingrowth of daughter nuclides, especially ^{241}Am arising from ^{241}Pu decay. Anyway, it appears that the highest increase in emitted dose rate over a 5 years period is obtained from plutonium with the III isotopic composition. The relative increase in total emitted dose rate is about 9.5 %, from 6.3 Gy s^{-1} to 6.9 Gy s^{-1}. Variations in emitted dose rate are given as additional data on table 10. Aging of plutonium samples in experiment presented below does not exceed 5 years so that the effect of dose rate changes can be neglected in first approximations.

2.2 - Synthesis

Plutonium dioxide samples were prepared using the conventional oxalic route. Stock plutonium dioxide samples were dissolved in nitric acid using HNO_3/HF under reflux. After dissolution, plutonium(VI) species were reduced using hydrogen peroxide. The Pu(IV) solutions were purified using anion exchange resin. Plutonium(IV) oxalate $Pu(C_2O_4)_2.6H_2O$ were precipitated by adding solid oxalic acid to plutonium(IV) nitric

solutions at room temperature under vigorous stirring. The precipitates were filtered and washed by water/ethanol (50/50) solution. The oxalate samples were calcined under air in a vertical furnace with a quartz insert. Temperature program consisted in an increase from ambient temperature to 110°C with 20°C/min rate. This temperature was hold for 1 hour to eliminate weakly bonded water. Then the furnace temperature was increased to the calcination temperature and hold for 6 hours. The furnace was then cooled down to ambient temperature. The described thermal cycle was performed three times on each sample although the plateau at 110°C was only performed during the first cycle. Calcination temperatures were set to the maximum values with the aim to obtain PuO_2 samples in a range of different specific surface area (SSA). Calcination temperatures were then set in the range of 450°C to 900°C. Plutonium dioxide specific surface area was obtained using the BET method on a Micromeretics Gemini 2375 apparatus. Analysis was performed only once on each sample due to the small quantity of these samples.

2.3 - Annealing treatments

Annealing treatments consisted in a 20°C/min ramp heating toward the desired temperature in air. Temperature was kept 50°C under sample's calcination temperature to prevent specific surface area shrinkage. The final temperature was hold for 5 hours. The sample is kept overnight under an air flow. The same procedure is then applied by substituting argon to air. The first cycle is operated under air to ensure oxidative treatment.

2.4 – Radiolysis experiments

Experiments consisted in contacting oxide sample with humid atmosphere inside gas tight glass cells. Relative humidity (RH) was imposed using lithium chloride solution based on equality of water activity in gas phase and solution. Lithium chloride solution is kept inside the vessel without contact with powder sample. Hydration is then induced by interaction between the humid gas phase and oxide surface. Radiolysis vessel is described in Figure 1. The use of glass for cells was motivated by its inability to catalyze reaction on its surface unlike stainless steel for example. The lowest part holds the oxide sample and the lithium chloride solution. The top is fitted with valves enabling filling and vacuum of the vessel as well as sampling line. Lithium chloride solution with the desired concentration is placed inside the solution holder. The solid sample is then put inside the cell as a thin layer (≈2 mm). This cell is tightly closed and undergoes series of vacuum and filling with conditioning gas to eliminate air traces. The cell was then backfilled with conditioning atmosphere and closed.

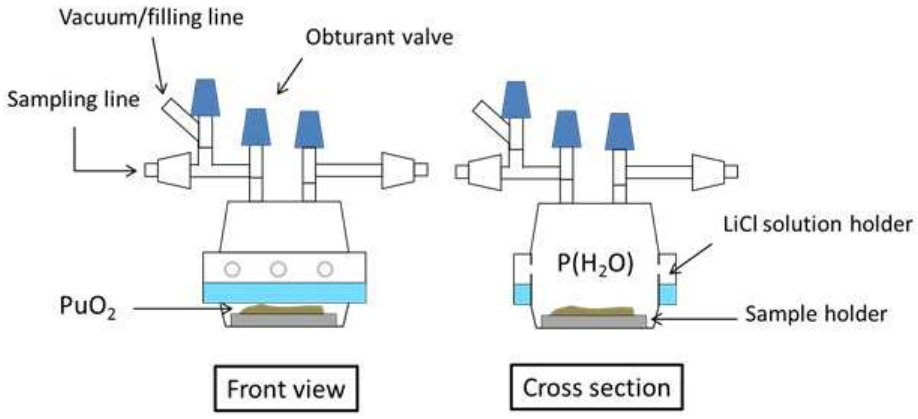

Figure 1 - Description of radiolysis cell. Approximate volume: 100mL, material: glass, inner solution: 2mL

Gas phase analysis was executed through the sampling line. This latter underwent series of vacuum and filling before analysis to eliminate air traces. Gas phase is analyzed by gas micro chromatography. Analyses were performed at regular intervals to record hydrogen generation kinetics, normalize to PuO_2 mass. The gas micro chromatograph was specifically designed to work inside plutonium materials gloveboxes. Sample inlet is provided by gas switching valve. Detection is executed by a thermal conductivity detector and the separation is obtained using a 5Å molecular sieve column. Carrier gas was argon. Neon is used as a tracer to obtain quantitative analysis. The instrument was calibrated using certified gas mixtures (He, H_2, O_2, N_2, Ne) supplied by Air Liquide company. Between experiments, radiolysis cells underwent series of vacuum and filling to renew the conditioning atmosphere.

The temperature inside the cell is assumed to be in equilibrium with the one of the glove-box. It is supported by the fact that all plutonium dioxides samples contain very small amount of ^{238}Pu (less than 50 mg) so that temperature increase due to ^{238}Pu decay can be neglected. The temperature inside the glove-box is maintained between 22 ° C and 26 °C.

3 - Results and Discussion

3.1 - Kinetics of hydrogen generation

The figure 2 shows typical experimental results for hydrogen accumulation induced by radiolysis of water adsorbed per mass of PuO_2 under argon atmosphere at 60% relative humidity. These results presented in figure 2 were obtained on oxide samples with isotopy II and isotopy I from Table 1. The hydrogen content increases linearly during the first hours of experiments. The existence of the steady state was systematically observed in the experiments regardless of plutonium isotopy, relative humidity or specific area. Sims *et al.* applied an analogue experimental device with constant humidity but did not observe steady state for the first 500 hours (Sims, 2013). The reach of hydrogen steady state suggests the existence of both hydrogen generation and

hydrogen consumption. The existence of an equilibrium value for hydrogen content was confirmed by conditioning radiolysis cell with hydrogen bearing atmosphere. Hydrogen evolution is shown in figure 3 and compared with hydrogen generation kinetics. Hydrogen content decreases constantly toward the equilibrium value observed in figure 2. The consumption of H_2 appears to follow a first order kinetic law. Both steady-state values obtained during H_2 accumulation and consumption show a good agreement (Figure 3).

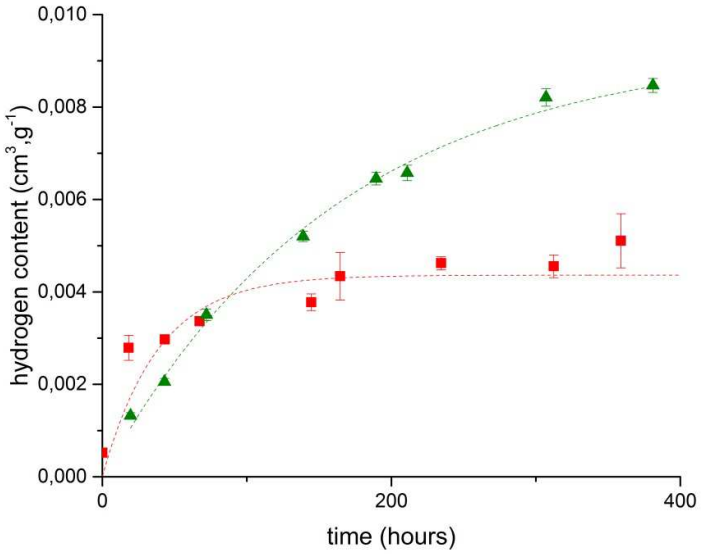

Figure 2 - Kinetics of hydrogen accumulation from radiolysis of adsorbed water normalized by PuO_2 mass (g). (■: accumulation atmosphere: argon, isotopy: II, SSA: 7.2 m^2 g^{-1}, RH=60%; ▲: accumulation atmosphere: argon, isotopy: I, SSA: 10.1 m^2 g^{-1}, RH=60%

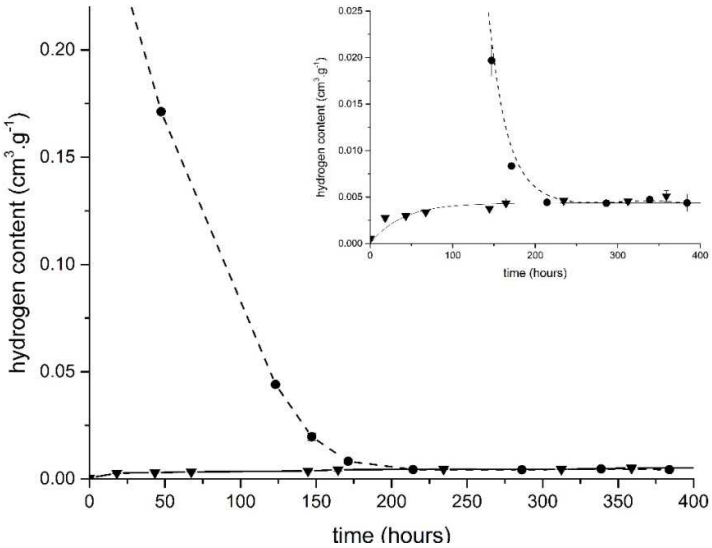

Figure 3 - Kinetics of hydrogen accumulation from radiolysis of adsorbed water normalized by PuO_2 mass (g) and consumption of hydrogen using hydrogen bearing atmosphere. (Conditions: isotopy II, SSA: 7.2 m^2 g^{-1}, RH=60%; accumulation (▼): argon atmosphere, consumption (●): argon/2000ppm H_2 atmosphere).

Thereby H_2 gas phase concentration at the steady state is resulting from an equilibrium between generation and consumption reactions. The initial rate R_0 and steady state content were determined by fitting the experimental data with a kinetic model. The kinetic model is based on a zero order kinetic law for generation (represented by R_0) and a first order kinetic law for consumption (represented by k) in (Eq. 10-11).

$$\frac{d[H_2]}{dt} = R_0 - k[H_2] \qquad \text{(Eq. 10)}$$

$$[H_2] = \frac{R_0}{k}\,(1 - \exp(-kt)) \qquad \text{(Eq. 11)}$$

The values of R_0 and k, and then the steady state content of H_2, $[H_2]_{stea.}$, can be determined from experimental kinetic curves of H_2 accumulation. For instance, in figure 2, the dashed curves are calculated with (Eq. 11) assuming R_0 and k values given in table 2.

Table 2 – Estimation of R_0 and k values for the calculated accumulation of H_2 on the basis of experimental data in figure 2

Sample	R_0 ($cm^3\ g^{-1}\ h^{-1}$)	k (h^{-1})	$[H_2]_{stea}$ ($cm^3\ g^{-1}$)
Ar ; Isotopy II ; SSA 7.2 $m^2.g^{-1}$; RH 60%	$1.59\ 10^{-4}$	$3.68\ 10^{-2}$	$4.31\ 10^{-3}$
Ar ; Isotopy I ; SSA 10.1 $m^2.g^{-1}$; RH 60%	$5.82\ 10^{-5}$	$6.25\ 10^{-3}$	$9.30\ 10^{-3}$

3.2 Influence of physical parameters on hydrogen generation kinetics

The influences of three different parameters were investigated: specific surface area (SSA), dose rate and relative humidity (RH). The influences of those parameters are first studied on initial rate of hydrogen generation (figure 4 and Table 3 to 6). Series of hydrogen generation experiments were performed to attempt the influence of one parameter at a time. However it might be difficult to obtain different samples with the same specific surface area and different dose rates.

The influence of specific surface area is detailed in Table 3. The table gives results of experiments performed on sample with isotopy III and within 80% relative humidity argon atmosphere. An increase of specific surface area leads to an increase of the initial rates. When the specific surface area is multiplied by almost 6, the initial rate increases only 3 times from 7.4 x 10^{-5} to 2.4 x 10^{-4} $cm^3\ g^{-1}\ h^{-1}$. The low specific surface area leads to a high uncertainty on the initial rate which is related to the low H_2 content close to analysis detection limit in the first hours of experiment (H_2 detection limit : 1 x 10^{-4} cm^3).

.

Table 3 - Evolution of initial rates of hydrogen generation according to specific surface area and relative humidity normalized by PuO_2 mass, (atmosphere: argon, isotopy: III).

Relative humidity (%)	Calcination temperature (°C)	SSA (m^{-2} g^{-1})	R_0 (cm^3 g^{-1} h^{-1})
80	900	2.0	$7.4 \times 10^{-5} \pm 5.3 \times 10^{-5}$
	700	4.6	$1.3 \times 10^{-4} \pm 0.3 \times 10^{-4}$
	600	11.8	$2.4 \times 10^{-4} \pm 0.8 \times 10^{-4}$
100	900	2.0	$1.1 \times 10^{-3} \pm 0.4 \times 10^{-3}$
	700	4.6	$1.5 \times 10^{-3} \pm 0.7 \times 10^{-3}$
	600	11.8	$3.6 \times 10^{-3} \pm 0.8 \times 10^{-3}$

The influence of relative humidity on initial rate is shown in Figure 4 and Table 4. These data show an important evolution when PuO_2 is placed in very high relative humidity atmosphere. The increase of the initial rate with relative humidity appears to be exponential between 60% and 100%. The influence of relative humidity was investigated on samples with different specific surface area and dose rate. The tendency is similar for all experiments. Relative humidity seems to be a crucial parameter for hydrogen generation. The influence of dose rate was experimentally more difficult to study because of the inability to obtain an exact reproducible surface area by calcination of precursor from different precipitation batches. Nevertheless, Figure 4 and Table 5 show a low dependency of the initial rate on specific surface area when relative humidity is equal to 60%.

Table 4 - Evolution of initial rates of hydrogen generation according to relative humidity normalized by PuO_2 mass (g). (argon atmosphere, isotopy: I, SSA: 10 m^2 g^{-1})

Relative humidity (%)	R_0 (cm^3 g^{-1} h^{-1})
60	$5.3 \times 10^{-5} \pm 1.1 \times 10^{-5}$
80	$1.5 \times 10^{-4} \pm 0.1 \times 10^{-4}$
100	$8.8 \times 10^{-4} \pm 1.9 \times 10^{-4}$

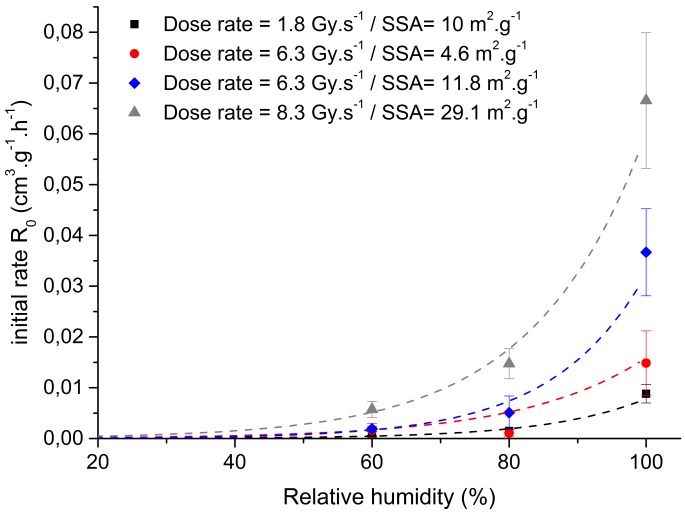

Figure. 4 - Dependency of initial rate of hydrogen generation with relative humidity normalized by PuO_2 mass. (argon atmosphere; ■: isotopy I, SSA=10 m^2 g^{-1} ; ● : isotopy III, SSA=4.6 m^2 g^{-1} ; ◆ : isotopy III, SSA=11.8 m^2 g^{-1} ; ▲: isotopy IV, SSA=29.1 m^2 g^{-1})

The influence of the dose rate on the initial rate of hydrogen generation was then investigated at 60% relative humidity. The results show an increase of the initial rate with the dose rate. The range of dose rates was 1.8 to 35.1 Gy s^{-1}. When the dose rate is multiplied by almost 20, the initial rate appears to be also multiplied by around 20. Table 6 shows a similar study performed at 100% relative humidity. Results show a similar tendency of increase of the initial rate with the dose rate. Increasing the dose rate leads to a higher decomposition of adsorbed water which could be explained by a higher absorbed energy. The initial rate related to radiolysis is then higher when the dose rate is higher (Table 5).

Table 5 - Evolution of initial rates of hydrogen generation according to dose rates normalized by PuO_2 mass (g). ***(argon atmosphere, relative humidity: 60%).***

Isotopy	Dose rate (Gy s^{-1})	SSA (m^2 g^{-1})	R_0 (cm^3 g^{-1} h^{-1})
I	1.8	7.4	$7.4 \times 10^{-6} \pm 5.3 \times 10^{-6}$
II	3.5	7.2	$1.1 \times 10^{-4} \pm 0.4 \times 10^{-4}$
III	6.3	6.3	$5.0 \times 10^{-4} \pm 1.1 \times 10^{-4}$
IV	8.4	29.1	$5.7 \times 10^{-4} \pm 1.6 \times 10^{-4}$
V	18.0	6.1	$8.2 \times 10^{-4} \pm 1.6 \times 10^{-4}$
VI	35.1	1.2	$16.2 \times .10^{-4} \pm 0.3.10^{-4}$

Table 6 - Evolution of initial rates of hydrogen generation according to dose rates (argon atmosphere, relative humidity: 100%)

Isotopy	Dose rate ($Gy.s^{-1}$)	SSA ($m^2.g^{-1}$)	R_0 ($cm^3.g^{-1}.h^{-1}$)
I	1.8	10.0	$8.8 \times 10^{-4} \pm 1.9 \times 10^{-4}$
III	6.3	11.8	$3.7 \times 10^{-3} \pm 0.9 \times 10^{-3}$

The influences of specific surface area, relative humidity and dose rate on steady state of hydrogen content were also studied. Steady state of hydrogen content appears less reproducible than initial rate. The tendency of the influences of the different parameters could be still determined. Table 7 gives results on steady state content of hydrogen and the influences of specific surface area, relative humidity and dose rate.

Table 7 - Variation of steady state hydrogen content with specific surface area, relative humidity and dose rates (argon atmosphere)

Isotopy	Dose rate ($Gy\ s^{-1}$)	SSA ($m^2\ g^{-1}$)	Relative humidity (%)	$[H_2]_{stat}$ ($cm^3\ g^{-1}\ h^{-1}$)
I	1.8	7.4	60	$1.7 \times 10^{-3} \pm 0.7 \times 10^{-3}$
II	3.5	7.2	60	$4.4 \times 10^{-3} \pm 0.4 \times 10^{-3}$
III	6.3	6.3	60	$7.0 \times 10^{-3} \pm 0.7 \times 10^{-3}$
III	6.3	28.7	60	$53.3 \times 10^{-3} \pm 17.5 \times 10^{-3}$
III	6.3	28.7	80	$209 \times 10^{-3} \pm 82 \times 10^{-3}$

Increasing relative humidity from 60% to 80% leads to an increase of the steady state content of hydrogen from 53.3×10^{-3} $cm^3\ g^{-1}$ to $209 \times .10^{-3} cm^3\ g^{-1}$. Increase in dose rate and specific surface area leads also to an increase of the steady state hydrogen content. However these last parameters appear to have a lower effect on the steady state than relative humidity.

Increase in specific surface area or relative humidity lead to an increase of both initial rate and steady state content. Initial rates (low hydrogen content) are more related to the radiolysis of sorbed water phenomenon while the steady state is related to both radiolysis of sorbed water and hydrogen consumption (high hydrogen content). The influences of specific surface area and relative humidity give information on both phenomena. The increase of specific surface area and relative humidity induces a similar effect of increasing the amount of water adsorbed on the surface. The first increases the surface accessible for water adsorption; the last increases the number of monolayers of water on the surface. Figure 4 shows an exponential increase of the initial rate over relative humidity. The shape of the curve is comparable with the shape of the water adsorption isotherm in the same range of relative humidity (Haschke, 1995). Literature suggests that each monolayer of water on surface has a different behavior toward radiolysis with important differences between the first monolayers (Laverne, 2003). Each monolayer can be seen as a specific generator of hydrogen. Adding monolayers might be considered as adding hydrogen generator. The steady state content is increasing with relative humidity and specific surface area (Table 7). Hydrogen consumption rate depends very likely on hydrogen content as suggested by equation 4. The equality of rates of hydrogen generation and hydrogen consumption might be attained at a higher value of hydrogen content when the initial rate is higher. Initial rate of hydrogen generation and steady state of hydrogen content are directly related.

Sims *et al.* implement a similar experimental set up with contacting PuO_2 samples with constant relative humidity atmosphere (Sims, 2013). H_2 generation kinetics appears linear over time. Sims *et al.* gives H_2 accumulation rates in the same order as the present study (Table 8) and gives a H_2 accumulation rate equal to 1.97 x $.10^{-3} cm^3 h^{-1} g^{-1}$ in the case of PuO_2 sample with a dose rate equal to 15.4 $Gy.s^{-1}$ and relative humidity equal to 95%. Sims *et al.* and Duffey *et al.* do not explain how dose rates are determined. The rates they reported in their studies were obtained under more extreme conditions (highest dose rate and highest relative humidity). Duffey *et al.* enclose PuO_2 samples with adsorbed water in closed vessel and monitored H_2 content after few days (Duffey, 2002). H_2 accumulation rates appear again in the same order than the present study but tend to be in the lower range of the present observations (Table 9). The maximum rate obtained was 42.1 x $10^{-5} cm^3 h^{-1} g^{-1}$ corresponding to PuO_2 sample with dose rate equal to 2.3 Gy s^{-1} and estimated water content equal to 4.1 wt.%. Duffey *et al.* were able to observe both H_2 and O_2 generation through adsorbed water radiolysis. For the highest H_2 generation, O_2 generation is close to half the generation of H_2. On the contrary, hydrogen generation is much lower than the one observed by Vladimirova *et al.* The existence of a final steady state was already observed (Vladimirova, 2002) at much higher value superior to 40 $cm^3.g^{-1}$ and was allocated to complete decomposition of adsorbed water. In this study, the physico-chemical system differs from the present study by the use of liquid water surface deposition. The deposition of liquid water on PuO_2 surface might not lead to an uniform film but rather drops. Physico-chemical configuration of water on surface might lead to higher hydrogen generation and water radiolysis in this case might be more similar to radiolysis of free water.

*Table 8 - Comparison of the average H_2 rate obtained in this work to the ones by Sims et al. *: Initial rates R_0.*

Relative humidity (%)	Dose rate (Gy s^{-1})	SSA ($m^2 g^{-1}$)	Average H_2 rate ($cm^3 g^{-1} h^{-1}$)	Ref.
95	4.6	8.9 ± 1.1	6.95 x 10^{-4} ± 3.8 x 10^{-5}	Sims, 2013
95	15.4	6.1 ± 1.0	1.97 x 10^{-3} ± 1.8 x 10^{-4}	Sims, 2013
80	28.7	6.3	2.4 x 10^{-4} ± 0.8 x 10^{-4}*	*this study*
100	28.7	6.3	3.6 x 10^{-3} ± 0.8 x 10^{-3}	*this study*

Table 9 - H_2 and O_2 accumulation rate obtained with another experimental methodology. (H_2 volume were calculated considering molar volume at 25°C and 1013 hPa)

Estimated H_2O content (%)	Dose rate (Gy s^{-1})	Calcination Temperature (°C)	H_2 rate ($cm^3 g^{-1} h^{-1}$)	O_2 rate ($cm^3 g^{-1} h^{-1}$)	Ref.
3	11.6	550	31.10^{-3}	3.10^{-3}	Vladimirova, 2002
3	1.9	550	5.10^{-3}	$0.6.10^{-3}$	Vladimirova, 2002
2.0	2.3	450	3.7 x 10^{-5} ± 0.2 x 10^{-5}	-8.4 x 10^{-5} ± 3.0 x 10^{-5}	Duffey, 2002
2.0	2.3	700	42.1 x 10^{-5} ± 3.9 x 10^{-5}	15.9 x 10^{-5} ± 3.9 x 10^{-5}	Duffey, 2002

3.3 Investigations on the origin of steady state

The existence of a steady state for H_2 generation implies equilibrium between generation and consumption. One can expect both H_2 and O_2 generation through adsorbed water radiolysis. Usually, oxygen is observed as a very low content. The Figure 5 shows the accumulation kinetics of both H_2 and O_2 during an experiment performed on PuO_2 samples with dose rate equal to 8.3 $Gy.s^{-1}$ and relative humidity equal to 100%. These conditions lead to a high generation of hydrogen through radiolysis. Dioxygen is also observed as is expected from decomposition of H_2O (Eq. 12).

$$H_2O \xrightarrow{\alpha} H_2 + \frac{1}{2}O_2 \qquad \text{(Eq. 12)}$$

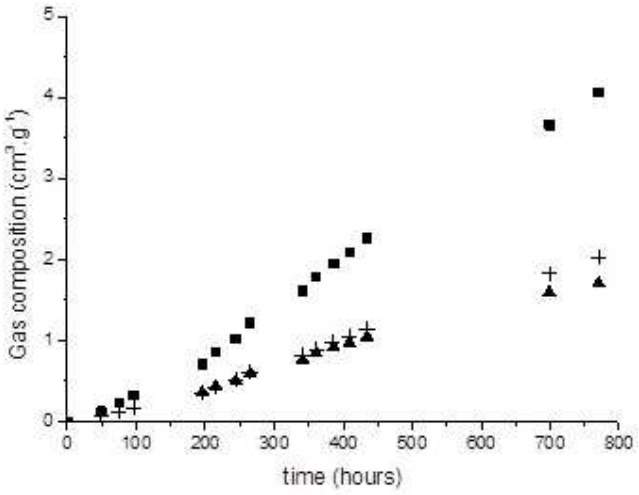

Fig. 5 - Evolution of hydrogen (■) and oxygen (▲) contents from radiolysis of water adsorbed on PuO_2.
(argon atmosphere, isotopy: III, RH=100% - crosses (+): expected oxygen content calculated from H_2 content (Eq.12))

Dioxygen is present in radiolysis cell as product of water radiolysis and trace amount from air traces. From the measure of nitrogen from air traces, dioxygen amount originated from air traces is calculated and subtracted to the measured amount of dioxygen. The calculated amount of dioxygen is meanly originated from water radiolysis. Expected oxygen content is calculated from H_2 content (shown by crosses in Figure 5). The expected values and the measured values appear to be in a good agreement with equation 12 and the ratio is close to 2. This result confirms that hydrogen and dioxygen generation is resulting from radiolysis of water. At low H_2 generation (low relative humidity, low dose rate for PuO_2), dioxygen is also generated but oxygen amount analysis is difficult. The range of dioxygen content cannot be efficiently analysed with the gas chromatograph used in this study. This might explain the low amount of dioxygen which is probably due to an analytical limitation (O_2 detection limit: 1 x 10^{-2} cm^3). Duffey *et al.* give a similar observation: O_2 generation is close to half the H_2 generation when H_2 content is high (Duffey, 2002).

The Figure 6 shows two H_2 generation kinetics obtained for the same conditions (isotopy VI and a RH of 60%). The second experiment was performed one year after the first one. The sample was kept in humid atmospheres

(water content was not kept constant) between experiments. Very high dose rate sample leads to a first high and quick generation of hydrogen and then to a decrease toward a steady state of hydrogen content. In both experiments, the consumption of H_2 appears to start at a certain H_2 overpressure but this pressure differs from one to the other. In the first experiment, the H_2 content begins to decrease when H_2 content is equal to 0.13 cm^3 x g^{-1}. In the second experiment the decrease begins at H_2 content equal to 0.09 cm^3 x g^{-1}. This experiment shows that the decrease of H_2 is not inferred by the H_2 content but another criterion is involved in the H_2 consumption mechanism. The aging of sample in H_2O/H_2 argon atmosphere during one year might lead to evolution of PuO_2 and especially its surface. The increase of H_2 in the first 4 days is in good agreement for both experiments. It can be concluded from this observation that the H_2 generation is not influenced by the evolution of PuO_2 sample over time contrary to the H_2 consumption. This observation is in accordance with Petrik's study (Petrik, 2001). Petrik *et al.* show that radiolysis of water in heterogeneous system is related to the solid electronic structure which is intrinsic of the solid nature. The evolution of the solid surface should not influence the radiolysis phenomena in the present heterogeneous system (adsorbed water/PuO_2).

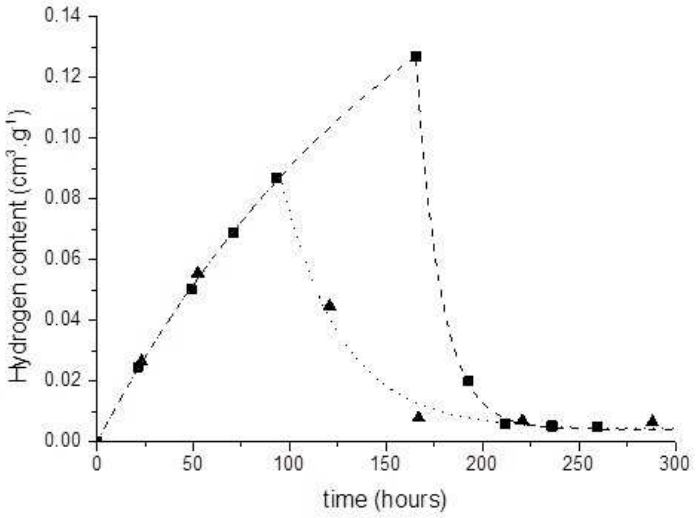

Fig. 6 - H_2 accumulation kinetics: evolution upon one year aging, ■: initial kinetics and ▲: aged (1 year later) (argon atmosphere, isotopy VI, RH 60%).

The Figure 7 shows different H_2 experiments performed with the same sample (PuO_2, isotopy III) at 80% relative humidity. The figure shows an initial kinetics performed with the sample as freshly prepared. A steady state is observed as in the other experiments. This sample was then kept in the radiolysis cell for almost 3 years to investigate the effect of aging sample in atmosphere containing H_2O (RH=80%) and H_2 through water radiolysis all along sample ageing. As in the previous case, after the long term aging, new hydrogen kinetics was performed to observe potential evolution of the steady state. The Figure 7 shows that the H_2 accumulation kinetics is significantly changed by aging. H_2 accumulation appears to be linear and no steady state was observed

in the 500 first hours. This observation is then in accordance with the study of Sims *et al.* where no steady state was observed (Sims, 2013).

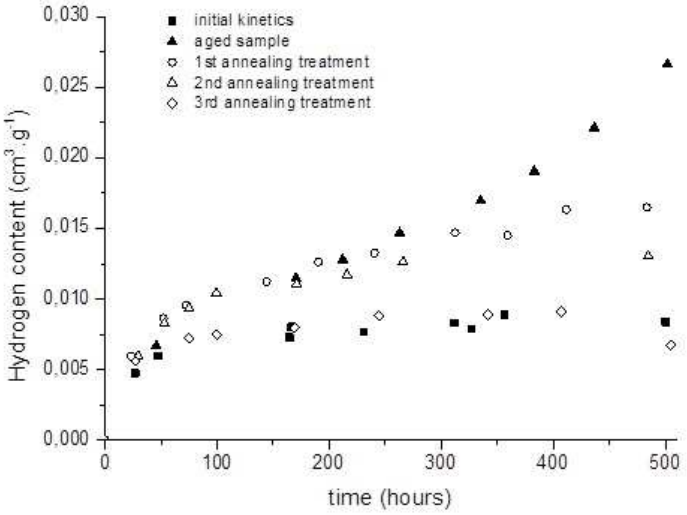

Fig. 7 - H_2 accumulation kinetics: variation upon three year aging and effect of annealing treatment (Atmosphere: argon, isotopy III, SSA=11.8 m^2 g^{-1}, RH=80%)

After that, surface evolution was investigated using annealing treatment. The annealing treatment consisted in heating the sample alternatively under air and argon during 5 hours at a temperature below calcination temperature by 50 °C to avoid any specific surface area shrinkage. Several identical annealing treatment were performed and H_2 accumulation kinetics was recorded after each treatment. Figure 7 shows the effect of successive annealing treatment. The first treatment leads to the back apparition of steady state after around 200 hours. The H_2 content at the steady state ($\approx 16.10^{-3}$cm^3 g^{-1}) appears to be higher than the one observed in the initial kinetics ($\approx 8.10^{-3}$ cm^3 g^{-1}). A second annealing treatment leads again to a steady state (13.10^{-3} cm^3.g^{-1}). This latter was lower than the one obtained after the first annealing treatment but still remains higher to the initial one. Finally, a third annealing treatment was performed and H_2 kinetics obtained after this latter is in good agreement with the initial one. For all H_2 kinetics, the initial rate does not change particularly (Figure 7). This latter one is mainly related to radiolysis of adsorbed water. As suggested by the result of the Figure 6, the phenomenon of H_2 generation through radiolysis of adsorbed water is not altered by the modification of PuO_2 surface. The H_2 consumption mechanism is on the contrary very much influenced by surface state of PuO_2. The storage of PuO_2 in humid atmosphere and hydrogen content might lead to a profound modification of PuO_2 surface and subsurface. The experiments described in Figure 7 indicate that annealing treatments lead to a progressive regeneration of the surface state. Not less than three annealing treatments under air and argon at high temperature (T=550°C) were needed to recover H_2 kinetics similar to the kinetics obtained on the sample as freshly prepared. This observation shows that the evolution of PuO_2 surface is severe and the recovery of initial PuO_2 surface is difficult. A long term storage in H_2O/H_2 conditions leads to an apparent absence of H_2 consumption. H_2 consumption seems to progressively reappear after annealing treatments.

3.4 Mechanism

These different observations lead to give some proposition on phenomena occurring during the experiment. The kinetic model relies on a zero order kinetic law for generation and a one order kinetic law for consumption. The steady state is the result of the equality of generation rate and consumption rate leading to steady state of H_2. H_2 generation rate is independent of H_2 content as shown by a constant R_0 (solid line Fig 8A). This latter depends solely on physical parameters as described above (isotopy, RH, SSA). On the contrary, H_2 consumption rate is then increasing linearly with H_2 partial pressure (dotted line Fig 8A). The consumption rate increases as H_2 accumulates in gas phase. At a certain H_2 content (P_a^{stat}, Fig 8A), the consumption rate becomes equal to the generation rate determining hydrogen steady state content $[H_2]_{stat}$. The experiments described in Figure 6 and Figure 7 suggest that generation is not changed by surface evolution and annealing treatment. The generation rate R_0 stays constant over surface evolution. On the opposite, consumption is more related to surface state. As shown in the Figure 7, H_2 consumption rate dependency might change with surface evolution. This leads to a shift of the steady state of hydrogen content toward higher values. This is represented on Figure 8B by lower and lower slope for H_2 consumption rate. This evolution of the consumption kinetics (decrease of $k[H_2]$) leads to an increase of the steady state of H_2 content (P_b^{stat} - Figure 8B). Another way to schematize these changes is drawn in Figure 9. Figure 9 was built using the expression (Eq. 11) assuming a constant value R_0 ($R_0 = 10^{-4}$ cm^3 g^{-1} h^{-1}) for H_2 production and decreasing k values. For the highest k values ($k = 6.25 \times 10^{-3}$ h^{-1} to 1.25×10^{-2} h^{-1}) a steady-state for H_2 content in the cell is clearly reached. This is consistent with the experimental result plotted on figure 2. As k value is decreasing ($k = 2.5 \times 10^{-3}$ h^{-1} to 1.25×10^{-3} h^{-1}), the steady state for H_2 content becomes higher and is reached only at longer time. For a low k value ($k = 1.25 \times 10^{-4}$ h^{-1}) which means that consumption of H_2 at the surface of the material becomes very slow, the variation of H_2 content as a function of time can even appear to be linear and no steady state seems to be reached. Actually, the experiment presented in Figure 7 with long term aging in H_2O/H_2 atmosphere show an absence of a steady state. This observation might be related to a drop in consumption rate. Consumption rate and generation rate would become equal at very high H_2 content. Sims *et al.* did not observe steady states of H_2 content (Sims, 2013). Authors do not specify the time between plutonium oxide synthesis and radiolysis experiments. According to the present observations, the absence of steady state might be explained by PuO_2 samples which were stored for an extended time between synthesis and experiments. In the present study, annealing treatments of aged PuO_2 surfaces appears to regenerate the surface and the ability to consume H_2. This observation indicates that the annealing treatment leads to an increase of the H_2 consumption kinetic constant. As shown on Figure 8C and Figure 9, this leads to a progressive lowering of H_2 steady state content (P_{cstat}).

The mechanism responsible for hydrogen consumption remains unknown but appears to be surface related. Hydrogen molecules must adsorb on the surface and dissociate. The dissociation might be implied by radiolysis but also by adsorption on oxide surface as observed on non-radioactive oxide (Linsebigler *et al.*, 1995). Dissociation products might have a strong reactivity toward the surface. Mechanisms explaining the steady state might be proposed based on surface redox chemistry of PuO_2. Hydrogen is known to have reductive properties. Formation of hydrogen might lead to reduction of surface and then consumption of hydrogen. The reactivity of water with PuO_2 surface is controversial. Formation of PuO_{2+x} was proposed by Haschke (Haschke, 2000), governing by the chemical surface reactivity of PuO_2 with water. In the present study, reduction of the surface by hydrogen could either cause the formation of substoichiometric phase PuO_{2-x} (PuO_2+Pu_2O_3) (Eq. 7) or reduction

of the superficial of the PuO_{2+x} phase toward stoichiometric surface or even further to substoichiometric surface (Eq. 8).

$$PuO_2 \underset{H_2}{\rightarrow} PuO_{2-x} \quad (7)$$

$$PuO_2 \underset{H_2O}{\longrightarrow} PuO_{2+x} \underset{H_2}{\rightarrow} PuO_2 \underset{H_2}{\rightarrow} PuO_{2-x} \quad (8)$$

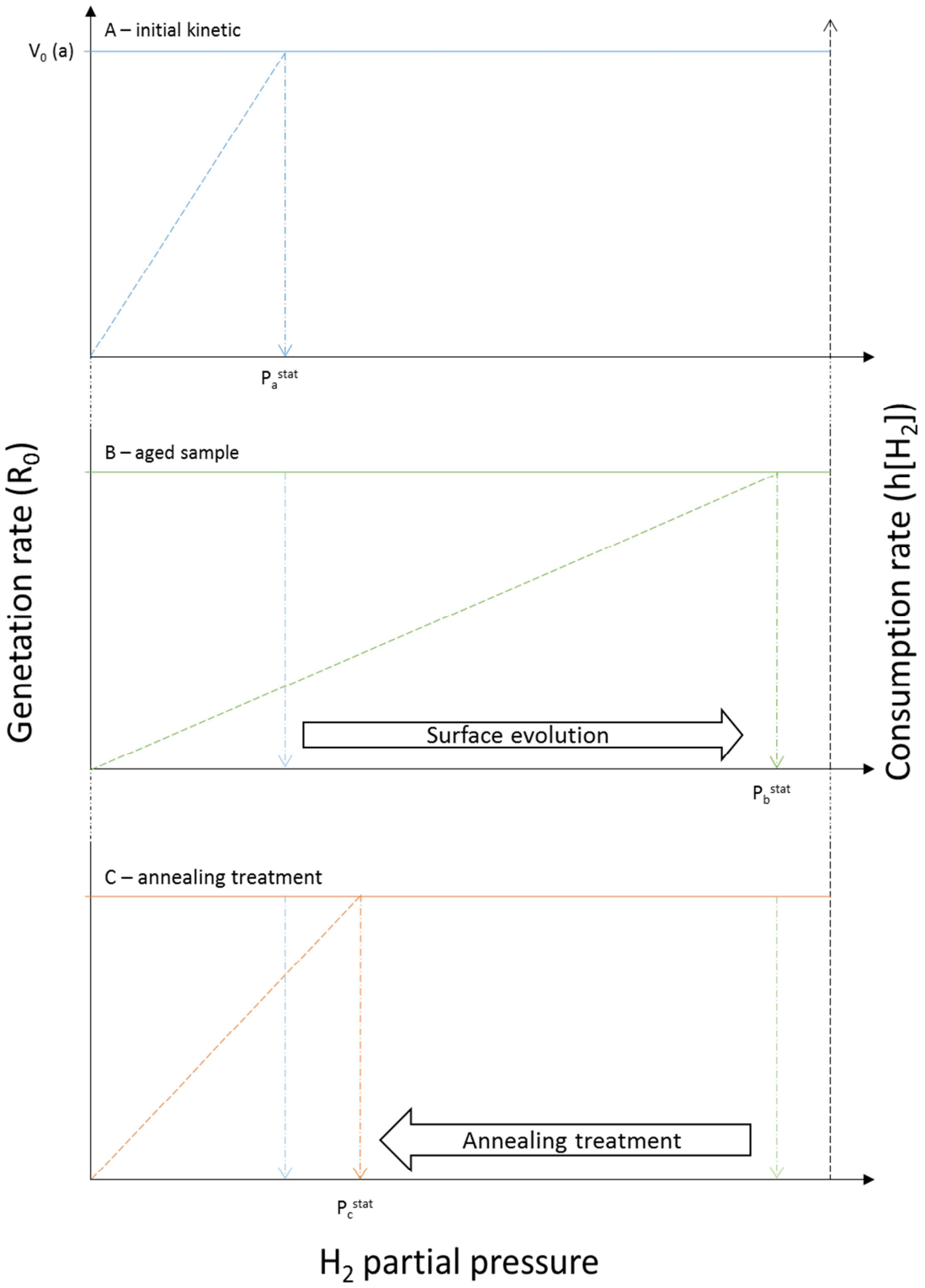

Fig. 8 – Comparison of H_2 formation and consumption rate as a function of H_2 content during radiolysis of sorbed water in different situations: variation of steady state H_2 content induced by consumption kinetics modification. (Atmosphere: argon, isotopy: III, SSA=11.8m^2 g^{-1}, RH=80%)

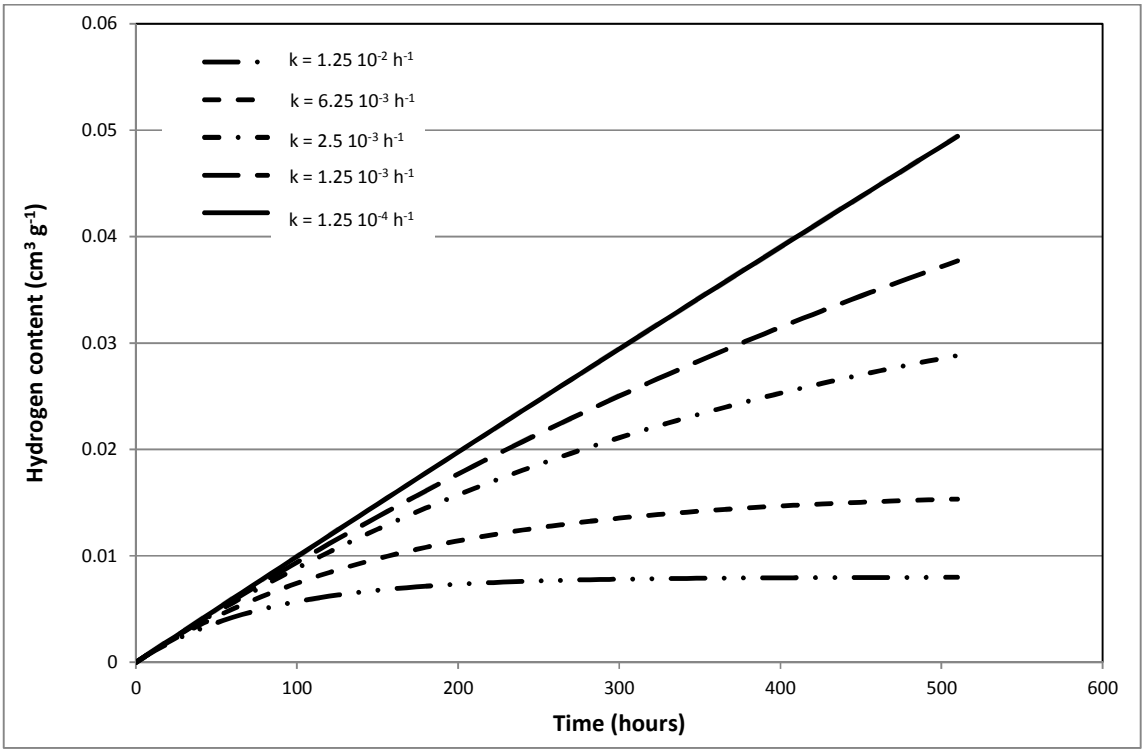

Fig. 9 – Modelling of H_2 accumulation in Ar atmosphere from the radiolysis of sorbed water on the basis of (Eq. 11) assuming a constant value for R_0 (10^{-4} cm^3 g^{-1} h^{-1}) and decreasing value for k due to the ongoing reduction of PuO_2 to PuO_{2-x} at the surface with the aging of the initial oxide

The reduction process might strongly depend on H_2 gas phase content. At certain H_2 content, the hydrogen generation rate through radiolysis and the consumption rate through redox chemistry would become equal leading to a steady state of hydrogen content. The fact that oxidative annealing treatments enables to progressively regenerate surface state supports a mechanism of surface progressive reduction implied by hydrogen over-pressure. The Figure 3 showing a consumption of hydrogen over-content brings information useful for mechanism investigation. The hydrogen over-pressure is consumed by a progressive reduction of the surface until the generation and consumption rates become equal. In the case of a long-term storage in H_2O/H_2 atmosphere, no steady state is observed. Hydrogen might migrate through surface to attain non reduced layer. Hydrogen is known to easily migrate in atomic sublayers (Senanayake *et al*, 2007). Hydrogen consumption mechanism might also be responsible of surface evolution over time in H_2O in closed radiolysis cell. The storage of 3 years might have led to a thick reduced layer preventing hydrogen migration toward a deep non reduced layer. Annealing treatment appears to restore the initial kinetics of hydrogen generation. Annealing treatment might allow regenerating progressively the surface state to PuO_2 stoichiometric surface.

4 - Conclusion

Radiolysis of water adsorbed on PuO_2 surface leads to hydrogen generation. The hydrogen content becomes constant after about some days. The hydrogen generation kinetics were characterized by the initial rate R_0 and the stationary content $[H_2]_{stat}$. Both initial rate and stationary content increases with specific surface area, relative

humidity and dose rate. A mechanism based on surface redox chemistry is proposed to explain the existence of the steady state and also surface evolution. The surface seems to be in a constant evolution which leads to an inhibition of the mechanism responsible for H_2 consumption. Oxidative annealing treatments lead to regenerate surface state altered by aging and restore the initial hydrogen generation kinetics. Physical parameters (specific surface area, relative humidity, dose rates) are not the only parameters governing the hydrogen accumulation. The surface state appears to be also a crucial parameter. The evolution of this latter in H_2O/H_2 atmosphere has to be more investigated and especially its impact on H_2 consumption reaction. This study underlines the importance of being able to investigate PuO_2 surface chemistry with non-intrusive technic to investigate mechanism occurring at the surface. In a previous work (Gaillard *et al.*, 2014) technics like Inverse Gas Chromatography (IGC), Raman Spectroscopy and Atomic Force Microscopy (AFM) enabled us to characterize the effect of hydration on ceria surface. XPS can be an interesting technic especially to investigate redox changes at the surface of plutonium. Unfortunately, most of these tools are not yet available in glove-box but a work is in progress to evaluate the feasibility of such study. A thought about the realization of experiments using ^{18}O- or D-labelled water or dihydrogen to get more information on a potential exchange mechanism at plutonium dioxide surface is in progress too.

Acknowledgments

This work was partly supported by the ORANO group and by the CEA into the Nuclear Energy Division in Research Department on Mining and Fuel Recycling Processes.

References

Alexandrov V., Shvareva T. Y., Hayun S., Asta M., Navrotsky A., 2011. Actinide. Dioxides in Water: Interactions at the Interface. Journal of Physical Chemistry Letters, 2(24):3130–3134.

Allen A. O., 1961. The radiation chemistry of water and aqueous solutions. Van Nostrand, Princeton, N.J.

Linsebigler A. L., Lu G., Yates J.T., 1995. Photocatalysis on TiO2 Surfaces: Principles, Mechanisms, and Selected Results. Chemical Reviews, 95(3):735–758.

Azimi G., Dhiman R., Kwon H., Paxson A. T., Varanasi K. K., 2013. Hydrophobicity of rare-earth oxide ceramics. Nature Materials, 12(4):315–320.

Benhamou A., Beraud Jp., 1980. Moisture Uptake by Plutonium Oxide Powder. Analusis, 8(8):376–380.

Duffey J. M., Livingston R. R., 2002. Gas generation testing of plutonium dioxide. 5th Topical DOE Spent Nuclear Fuel and Fissile Materials Management, page 6 pp.

Gaillard J., Venault L., Calvet R., Del Confetto S., Clavier N., Podor R., Odorico M., Pellequer J. L., Vigier N., Moisy P., 2014, Effect of hydration and thermal treatment on ceria surface using non-intrusive techniques, Journal of Nuclear Materials, 444, 359-367

Haschke J. M., Ricketts T. E., 1995. Plutonium dioxide storage: Conditions for preparation and handling.

Hascke J. M., Ricketts T. E., 1997. Adsorption of water on plutonium dioxide, Journal of Alloys and Compounds, 252, 148-156

Haschke J. M., Allen T. H., Morales L. A., 2000. Reaction of plutonium dioxide with water: Formation and properties of PuO_{2+x}. Science, 287(5451):285–287.

Haschke J. M., Allen T. H., Morales L. A., 2001. Reactions of plutonium dioxide with water and hydrogen-oxygen mixtures: Mechanisms for corrosion of uranium and plutonium. Journal of Alloys and Compounds, 314(1-2):78–91.

Hodkin D.J., Pitman R.S., Mardon P.G., 1965. Gas evolution from solid plutonium-bearing residues during storage.

LaVerne J. A., Pimblott S. M., 2000. New Mechanism for H_2 Formation in Water. The Journal of Physical Chemistry A, 104(44):9820–9822.

LaVerne J. A., Tandon L., 2002. H_2 production in the radiolysis of water on CeO_2 and ZrO_2. Journal of Physical Chemistry B, 106(2):380–386.

LaVerne J. A., Tandon L., 2003. H_2 Production in the Radiolysis of Water on UO_2 and Other Oxides. The Journal of Physical Chemistry B, 107(49):13623–13628.

McNeilly C. E., 1964. The electrical properties of plutonium oxides. Journal of Nuclear Materials, 11(1):53–58.

Petrik N. G., Alexandrov A. B., Vall A. I., 2001. Interfacial Energy Transfer during Gamma Radiolysis of Water on the Surface of ZrO_2 and Some Other Oxides. The Journal of Physical Chemistry B, 105(25):5935–5944.

Sims H. E., Webb K. J., Brown J., Morris D., Taylor R. J., 2013. Hydrogen yields from water on the surface of plutonium dioxide. Journal of Nuclear Materials, 437(1-3):359–364.

Stakebake J. L, Steward L. M., 1973. Water vapor adsorption on plutonium dioxide. Journal of Colloid and Interface Science, 42(2):328–333.

Senanayake S. D., 2007, Waterhouse G. I. N., Chan A. S. Y., Madey T. E., Mullins D. R., Idriss H., 2007. The reactions of water vapour on the surfaces of stoichiometric and reduced uranium dioxide: A high resolution XPS study. Catalysis Today, 120(2):151–157.

Vladimirova M. V., Kulikov I. A., 2002. Formation of H_2 and O_2 in Radiolysis of Water Sorbed on PuO_2. Radiochemistry, 44(1):86–90.

Supplementary Data

Table 10 - LNHB data for alpha energies and specific activities for plutonium isotopes.

	^{238}Pu	^{239}Pu	^{240}Pu	^{241}Pu	^{242}Pu	^{241}Am
$A_\alpha(10^{14}$ Bq.kg$^{-1})$	6.333	0.021	0.084	--	0.001	1.270
$E_\alpha(10^{-16}$ J)	8.8	8.3	8.3	--	7.8	8.9
$A_\beta(10^{14}$ Bq.kg$^{-1})$	--	--	--	38.11	--	--
$E_\beta(10^{-16}$ J)	--	--	--	0.03	--	--

Table 11 – Variations of isotopic composition and total emitted dose rate

Isotopy	^{238}Pu	^{239}Pu	^{240}Pu	^{241}Pu	^{242}Pu	^{241}Am	Dose rate (Gy.s^{-1})
I	--	96.92	2.98	0.03	0.08	--	1.8
I aged 5 years	--	96.91	2.98	0.02	0.08	0.01	1.8
II	0.17	76.51	21.23	1.41	0.68	--	3.5
II aged 5 years	0.16	76.52	21.22	1.11	0.68	0.30	3.8
III	0.69	70.14	22.33	3.86	2.98	--	6.3
III aged 5 years	0.66	70.17	22.33	3.06	2.98	0.82	6.9
IV	1.07	67.74	22.39	4.68	4.12	--	8.3
IV aged years	1.03	67.78	22.39	3.68	4.12	1.00	8.9
V	3.08	66.42	21.93	4.49	4.15	--	18.0
V aged 5 years	2.85	66.55	21.96	2.78	4.16	1.70	18.3
VI	6.58	64.08	21.01	4.20	4.18	--	35.0
VI aged 5 years	6.11	64.39	21.09	2.61	4.20	1.60	34.7